Quantum Chemical and Theoretical Kinetics Study of the O(3 P) + C 2 H 2 Reaction: A Multistate Process †

3 AUTHORS, INCLUDING:

Thanh Lam Nguyen
University of Texas at Austin
72 PUBLICATIONS **1,384** CITATIONS

SEE PROFILE

Jozef Peeters
University of Leuven
205 PUBLICATIONS **4,473** CITATIONS

SEE PROFILE

Quantum Chemical and Theoretical Kinetics Study of the O(^{3}P) + C$_2$H$_2$ Reaction: A Multistate Process[†]

Thanh Lam Nguyen, Luc Vereecken, and Jozef Peeters*

Department of Chemistry, University of Leuven, Celestijnenlaan 200F, B-3001 Leuven, Belgium

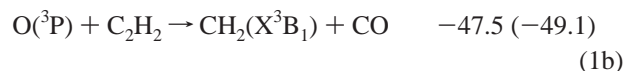*Received: October 18, 2005; In Final Form: February 13, 2006*

The potential energy surfaces of the two lowest-lying triplet electronic surfaces ^{3}A″ and ^{3}A′ for the O(^{3}P) + C$_2$H$_2$ reaction were theoretically reinvestigated, using various quantum chemical methods including CCSD-(T), QCISD, CBS-QCI/APNO, CBS-QB3, G2M(CC,MP2), DFT-B3LYP and CASSCF. An efficient reaction pathway on the electronically excited ^{3}A′ surface resulting in H(^{2}S) + HCCO(A^{2}A′) was newly identified and is predicted to play an important role at higher temperatures. The primary product distribution for the multistate multiwell reaction was then determined by RRKM statistical rate theory and weak-collision master equation analysis using the exact stochastic simulation method. Allowing for nonstatistical behavior of the internal rotation mode of the initial ^{3}A″ adducts, our computed primary-product distributions agree well with the available experimental results, i.e., ca. 80% H(^{2}S) + HCCO(X^{2}A″ + A^{2}A′) and 20% CH$_2$(X^{3}B$_1$) + CO-(X$^1\Sigma^+$) independent of temperature and pressure over the wide 300–2000 K and 0–10 atm ranges. The thermal rate coefficient k(O + C$_2$H$_2$) at 200–2000 K was computed using multistate transition state theory: $k(T) = 6.14 \times 10^{-15} T^{1.28} \exp(-1244 \text{ K}/T)$ cm^3 molecule^{-1} s^{-1}; this expression, obtained after reducing the CBS-QCI/APNO ab initio entrance barriers by 0.5 kcal/mol, quasi-perfectly matches the experimental $k(T)$ data over the entire 200–2000 K range, spanning 3 orders of magnitude.

I. Introduction

Chemical processes occurring in combustion and flames go through complex reaction networks normally consisting of several hundreds and even thousands of coupled elementary reactions occurring consecutively and/or in parallel. Characterizing the dominant elementary reactions is very important to understand the overall reaction mechanisms as well as to optimize the combustion process. Acetylene is known to be a major intermediate in almost all hydrocarbon-fueled flames.[1] Also, it is well established that the major consumption pathway of acetylene is reaction with an oxygen atom in its electronic triplet ground state.[2] This reaction plays an important role in hydrocarbon combustion chemistry because it leads to several highly reactive small radicals such as HCCO, triplet and singlet CH$_2$, H, CH and C$_2$H. Some of those can successfully attack closed-shell molecules such as C$_2$H$_2$ and even N$_2$, or react further with other atoms or radicals in highly exothermic reactions, thus causing major flame phenomena such as chemi-ionization and chemiluminescence, prompt-NO formation and production of PAH- and soot precursors.[2]

Experimental[3–12] and theoretical[13,14] studies agree that the primary products of the O(^{3}P) + C$_2$H$_2$ reaction are produced through two channels, as presented below. Experimental reaction enthalpies[15] ($\Delta_r H$(0 K), in kcal/mol) are given, whereas the values in parentheses are obtained by us using quantum chemical calculations at the CCSD(T)/6-311++G(3df,2p) + ZPE[CCSD-

(T)/6-311++G(d,p)] level of theory (vide infra).

$$O(^3P) + C_2H_2 \rightarrow H(^2S) + HCCO(X^2A'')$$
$$-19.7 \ (-19.6) \quad (1a)$$

$$O(^3P) + C_2H_2 \rightarrow CH_2(X^3B_1) + CO \quad -47.5 \ (-49.1)$$
$$(1b)$$

It should be mentioned that the hydrogen abstraction channel (O(^{3}P) + C$_2$H$_2$ → OH(X^2′) + HCC(X$^2\Sigma$)) is so highly endothermic ($\Delta_r H$(0 K) $\approx$ 31 kcal/mol; see Table 1) that it cannot compete with the addition/elimination routes, even at T = 3500 K. As a result, the abstraction is unimportant under all combustion conditions.

The product branching ratio for the O(^{3}P) + C$_2$H$_2$ reaction was a subject of controversy for a long time, as detailed in some more recent work.[2,7,11] Suffice it to mention here that in some early work the minor channel (1b) was thought to be the dominant one. However, all recent experimental determinations, by Michael et al.[7] and by us[8,9] agree that the products H(^{2}S) + HCCO are predominant over CH$_2$(X^{3}B$_1$) + CO, with the yield of the former being 80 ± 10% and nearly independent of temperature for T = 290–1200 K. These results were reconfirmed very recently in molecular beam experiments by Casavecchia et al.[11] for collision energies of 9.5 kcal/mol. The product distribution for this reaction was theoretically computed earlier by Harding and Wagner,[14] with the yield for products H(^{2}S) + HCCO(X^{2}A″) predicted to be 70^{+10}_{-35}%, closely forecasting the more recent experimental results mentioned. These theoretical calculations were based on an approximate potential energy surface constructed mainly at the CISD+Q level of

Kinetics Study of the O(^{3}P) + C$_2$H$_2$ Reaction

J. Phys. Chem. A, Vol. 110, No. 21, 2006 **6697**

TABLE 1: Computed Relative Energy (kcal/mol) at $T = 0$ K for Species in the O(^{3}P) + C$_2$H$_2$ Reaction Using the CBS-QCI/APNO and CCSD(T)/6-311++G(3df,2p) Levels of Theory[a]

species	CBS-QCI/APNO	CCSD(T)-1[b]	exptl[c]	CISD+Q[d]	BAC-MP4[d]	estimation[d]	CCSD(T)[e]
O(^{3}P) + C$_2$H$_2$	0.0	0.0	0.0	0.0	0.0	0.0	0.0
H(^{2}S) + HCCO(X^{2}A″)	−20.7	−19.6	−19.7	−8.6	−18.7	19.1 ± 2.5	
H(^{2}S) + HCCO(A^{2}A′)		−16.5					
CH$_2$(X^{3}B$_1$) + CO	−47.7	−49.1	−47.5	−47.4	−50.6	−46.9 ± 0.5	
CH$_2$(a^{1}A$_1$) + CO	−39.0	−39.4	−38.5				
OH(X^2′) + HCC(X^{2}Σ$_g$)	31.9	31.9	30.4				
HC(X^2′) + HCO(X^{2}A′)	36.9	35.9	38.4				
H$_2$ + CCO(X^{3}Σ$_g$)	−24.6	−24.7	−22.4				
ketene, H$_2$CCO(C$_{2v}$,X^{1}A$_1$)	−125.6	−122.4	−124.2				−121.7
Int1(C$_s$,^{3}A″), *trans*-OC$_2$H$_2$	−51.7	−50.6		−45.9	−50.1	−59.5 ± 5	−52.0
Int2(C$_s$,^{3}A″), *cis*-OC$_2$H$_2$	−50.4	−49.1				−58.7 ± 5	−50.8
Int3(C$_s$,^{3}A″), H$_2$CCO	−71.4	−69.2		−63.1	−69.2	−75.9 ± 4	−72.4
TS1(C$_s$,^{3}A″)	3.5	5.3		11.7	8.4	3.3	
TS2(C$_s$,^{3}A″)	31.7^g						
TS3(C$_1$,^{3}A)	−46.0	−44.7			−45.2		−45.1
TS4(C$_s$,^{3}A″)	−9.5	−7.1					
TS5(C$_1$,^{3}A)	−10.4	−7.8		2.0	−5.6	−15.6 ± 5	−7.0
TS6(C$_s$,^{3}A″)	−16.6	−14.8		−0.2	−11.4	−16.1 ± 5	
TS7(C$_1$,^{3}A)	−2.5	0.3					
TS8(C$_s$,^{3}A″)	−44.2	−43.9		−39.3		−42.0 ± 2	
Int1-ex(C$_s$,^{3}A′)	−22.5	−21.0		−18.5		−32.1 ± 5	
Int2-ex(C$_s$,^{3}A′)	−23.2						
TS1-ex(C$_s$,^{3}A′)	6.1^f			15.9		6.3 ± 1.3	
TS3-ex(C$_s$,^{3}A′)	−21.2	−20.3					
TS6-ex(C$_s$,^{3}A′)	−5.0	−4.2					

a The available experimental data and values in the literature are given for the purpose of comparison. *b* CCSD(T)/6-311++G(3df,2p)//CCSD(T)/6-311++G(d,p) + ZPE[CCSD(T)/6-311++G(d,p)]. *c* Mainly taken from the web-page http://srdata.nist.gov/cccbdb/. All values were obtained at 0 K: $\Delta H^0_f(0) = 58.98$ kcal/mol; $\Delta H^0_f(C_2H_2) = 54.48$ kcal/mol; $\Delta H^0_f(H) = 51.63$ kcal/mol; $\Delta H^0_f(HCCO) = 42.0$ kcal/mol;[67] $\Delta H^0_f(CH_2(X^3B_1)) = 93.2$ kcal/mol; $\Delta H^0_f(CH_2(a^1A_1)) = 102.2$ kcal/mol; $\Delta H^0_f(CO) = -27.2$ kcal/mol; $\Delta H^0_f(OH) = 8.84$ kcal/mol; $\Delta H^0_f(HCC) = 135.0$ kcal/mol; $\Delta H^0_f(HC) = 141.98$ kcal/mol; $\Delta H^0_f(HCO) = 9.95$ kcal/mol; $\Delta H^0_f(CCO(X^3\Sigma_g)) = 91.1$ kcal/mol;[68] $\Delta H^0_f(H_2CCO) = -10.66$ kcal/mol. *d* Reference 14. *e* Reference 23. *f* Derived from the G2M(CC,MP2) approach, CBS-QCI[TS1-ex] = CBS-QCI[TS1] + {G2M[TS1-ex] − G2M[TS1]} = 3.5 + {7.2 − 4.6} = 6.1. *g* This value = (G2M + CBS-QB3 + G3 + G3B3)/4 (see Table S7 in the Supporting Information).

theory but modified to match some experimental enthalpies.[14] Considering the accuracies obtainable with current quantum chemical methods such as the coupled-cluster theory[16] and the combination methods (Gaussian-3 theory (G3),[17] complete basis set (CBS)[18] model chemistry), a thorough reinvestigation of the potential energy surface for the O(^{3}P) + C$_2$H$_2$ reaction from first principles appears to be in order.

Thermal rate coefficients for the reaction of ground-state atomic oxygen with acetylene were measured over a wide range of temperature:[21] e.g., at low $T = 200-284$ K by Bohn and Stuhl,[19] at moderate T by Sheaffer and Zittel (295−873 K),[20] among many others, and at higher $T = 290-1510$ K by Mahmud and Fontijn[5] as well as at $T = 850-1950$ K by Michael and Wagner.[7] From these reports, the experimental Arrhenius activation energy is derived to be about 3−3.5 kcal/mol. At room temperature, the thermal rate coefficient is well-known to be ∼1.4 × 10^{-13} cm^3 molecule^{-1} s^{-1}.[21] Overall thermal rate coefficients were theoretically computed using conventional transition state theory (TST) adopting the experimental activation energy of 3.3 kcal/mol.[7,14] In these studies, theory and experiment were in good agreement at temperatures below 1000 K, though the predicted rates were about 2 times lower than observed in high-temperature shock tube experiments. The reason for this discrepancy was not clear.[7,14]

Theoretical ab initio quantum chemical investigations of the potential energy surface of the O(^{3}P) + C$_2$H$_2$ reaction are few. As mentioned above, Harding et al.[13,14] investigated the two lowest-lying triplet surfaces as part of his theoretical kinetic work, qualitatively elucidating the reaction mechanism as well as showing the predominance of channel 1a over channel 1b. Some stationary points on the triplet PES were characterized using the BAC-MP4 method[22] and the CCSD(T)/cc-pVTZ//B3LYP/6-31G(d,p) level of theory.[23] However, the triplet surfaces clearly need to be refined further to gain energies with sufficient accuracy for accurate kinetic calculations, in particular to investigate higher-energy pathways that might clear up the underestimation of the predicted rate coefficient at higher temperatures. Considering the paramount importance of the reaction of acetylene with atomic oxygen in hydrocarbon combustion and flames, we set out to reinvestigate this reaction using coupled-cluster theory and the CBS-QCI/APNO combination method to construct the two lowest-lying triplet surfaces, and to use these in high-level theoretical kinetic analyses. The computed results will then be compared with the available experimental data.

II. Methodology

II. 1. Quantum Chemical Calculations. Geometries and Hessians of stationary points were obtained first at the DFT-B3LYP/6-311G(d,p) level of theory[24,25] and then used as initial guesses for optimizing at the coupled-cluster level of theory [CCSD(T)][26] in combination with the 6-311++G(d,p) basis set.[27] Numerical Hessian calculations were carried out at the same level to verify the stationary points located (one imaginary frequency for a transition structure and all positive frequencies for a minimum) and to obtain zero-point vibrational energies (ZPE) and harmonic vibrational frequencies. To obtain more accurate relative energies, the CCSD(T) method in combination with the much larger extended 6-311++G(3df,2p) basis set[27] was employed to compute single-point energies. Note that the ZPE[CCSD(T)] are used unscaled to correct the relative energies.

For some stationary points that influence the reaction kinetics strongly, the effect of basis set size on the optimized geometries and energies was also investigated by reoptimizing at larger

TABLE 2: Computed Relative Energy (kcal/mol) for Some Stationary Points That Kinetically Control the O(^{3}P) + C$_2$H$_2$ Reaction Using Various Levels of Theory

species	G2M(CC,MP2)[a]	CBS-QCI/APNO[b]	CCSD(T)-1[c]	CCSD(T)-2[d]	CCSD(T)-3[e]
O(^{3}P) + C$_2$H$_2$	0.0	0.0	0.0	0.0	0.0
Int1(C$_s$,^{3}A″)	−51.3	−51.7	−50.6	−51.1	−50.2
TS1(C$_s$,^{3}A″)	4.6	3.5	5.3	5.2	5.9
TS1-ex(C$_s$,^{3}A′)	7.2				
TS4(C$_s$,^{3}A″)	−8.4	−9.5	−7.1	−7.1	−6.9
TS5(C$_1$,^{3}A)	−9.3	−10.4	−7.8	−8.4	−8.0
TS6(C$_s$,^{3}A″)	−16.2	−16.6	−14.8	−14.7	−14.2
TS7(C$_1$,^{3}A)	−1.2	−2.5	0.3	−0.4	0.3

[a] G2M(CC,MP2) = CCSD(T)/6-311++G(d,p) + [MP2/6-311++G(3df,2p) − MP2/6-311++G(d,p)] + ZPE[B3LYP/6-311++G(3df,2p)], based on the B3LYP/6-311++G(3df,2p) optimized geometry. [b] Replacing the corrected ZPE[HF] in the original CBS-APNO approach by the ZPE obtained at the QCISD/6-311G(d,p) level and scaled down by 0.9776.[69] [c] CCSD(T)-1 = CCSD(T)/6-311++G(3df,2p)//CCSD(T)/6-311++G(d,p) + ZPE[CCSD(T)/6-311++G(d,p)]. [d] CCSD(T)-2 = CCSD(T)/6-311++G(3df,3pd)//CCSD(T)/6-311++G(2df,2pd) + ZPE[CCSD(T)/6-311++G(d,p)]. [e] Extrapolating the CCSD(T) approach to an infinite basis set using energies at the CCSD(T)/cc-pCVQZ and CCSD(T)/cc-pCVTZ levels based on the CCSD(T)/cc-pVTZ optimized geometry. CCSD(T)-3 = HF/cc-pCVQZ + E_{corr} + ZPE[CCSD(T)/6-311++G(d,p)], where E_{corr} = {$4^3 E_{corr}$(cc-pCVQZ) − $3^3 E_{corr}$(cc-pCVTZ)}/{$4^3 − 3^3$}, and CCSD(T)/cc-pCVQZ ≈ CCSD(T)/cc-pCVTZ + [MP2/cc-pCVQZ − MP2/cc-pCVTZ].

basis sets such as 6-311++G(2df,2pd) or cc-pVTZ,[27] followed by single-point CCSD(T) energy calculations using the 6-311++G(3df,3pd) basis set or an extrapolation to a basis set limit, respectively. For the extrapolations, cc-pCVTZ and cc-pCVQZ[27] basis sets were employed:[28]

$$E_{limit}^{CCSD(T)} = E_{cc-pCV(TQ)Z}^{CCSD(T)} = E_{cc-pCVQZ}^{HF} + E_{cc-pCV(TQ)Z}^{corr} \quad (2)$$

where

$$E_{cc-pCV(TQ)Z}^{corr} = \frac{E_{cc-pCVQZ}^{corr} \times 4^3 - E_{cc-pCVTZ}^{corr} \times 3^3}{4^3 - 3^3}$$

with

$$E_{cc-pCVQZ}^{corr} = E_{cc-pCVQZ}^{CCSD(T)} - E_{cc-pCVQZ}^{HF}$$

and

$$E_{cc-pCVTZ}^{corr} = E_{cc-pCVTZ}^{CCSD(T)} - E_{cc-pCVTZ}^{HF}$$

Because of the limitations of our current computational resources, we could not do single-point energy calculations at the CCSD(T)/cc-pCVQZ level. We therefore approximated energies at this level by a linear extrapolation using the MP2/cc-pCVQZ level[29,30] with an additive scheme presented as follows:

CCSD(T)/cc-pCVQZ = CCSD(T)/cc-pCVTZ + [MP2/cc-pCVQZ − MP2/cc-pCVTZ]

The relative energies, tabulated in Table 2, computed at the CCSD(T) level using three different basis sets for the important stationary points, are in excellent agreement with each other, i.e., a discrepancy of only ∼0.5 kcal/mol and little sensitivity to the basis set used, indicating that the computed relative energies in this work are nearly converged.

Additionally, various combination methods such as CBS-QCI/APNO,[18] CBS-QB3,[31] G3B3,[32] G3,[17] and G2M(CC,MP2)[33] were applied for the purpose of comparison with the direct coupled-cluster calculations. All relative energies computed using these methods, presented in Table S7 (see the Supporting Information), agree well each other. We chose the CBS-QCI/APNO approach to compare with the CCSD(T) results and for kinetic calculations, as this level is thought to be the best in this series of CBS family. Note that we modified the original CBS-QCI/APNO approach by replacing the HF-ZPE with the QCISD-ZPE correction, as suggested earlier by Radom et al. for radical

systems.[34] Table 1 shows that the CBS-QCI/APNO results are in good agreement with the CCSD(T) values and also with the available experimental data. However, a discrepancy of ∼1 kcal/mol as compared to experiment still remains for fragment radicals, for which heats of formation have an uncertainty of ±1 kcal/mol, or even higher.[15]
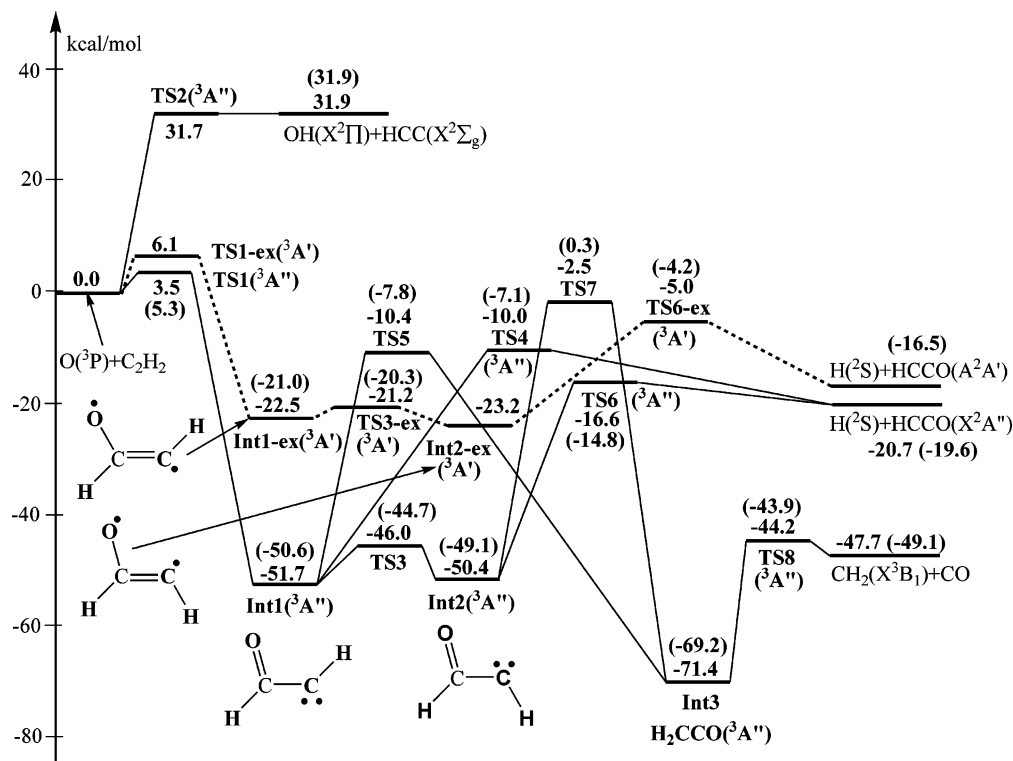
To check the effects of multiconfiguration or near-degeneracies of the wave functions for stationary points and particularly for the transition structures, we reoptimized all stationary points in Figure 1 using the CASSCF(8,8)/6-311++G(d,p) level of theory[35,36] and performing analytical Hessian calculations as well. The CASSCF calculations confirmed that for each of the species considered in this paper (see the Supporting Information) the HF-wave function is dominant (i.e., the CI-coefficient of the most important configuration is >0.9), indicating that a single-reference method should give fair results in all cases. Finally, intrinsic reaction coordinate (IRC)[37,38] calculations were done at the B3LYP/6-311G(d,p) level to establish the correct connections between the reaction intermediates; all IRC calculations are given in Figures S9−S16 in the Supporting Information.

The CCSD(T), QCISD, CBS-QCI/APNO, DFT-B3LYP, G2M(CC,MP2), CBS-QB3, G3B3, and G3 calculations were performed using the Gaussian 03 package,[39] whereas the CASSCF geometries and vibrational frequencies were computed using the Dalton[40] and Molpro[41] packages. All optimized geometries, harmonic vibrational frequencies, rotational constants, and energies are given in the Supporting Information.

II.2. RRKM/Master Equation Calculations. Product distributions as a function of temperature and pressure ($P ≤ 1$ atm, $T = 298-2000$ K) for the O(^{3}P) + C$_2$H$_2$ reaction proceeding on the adiabatic triplet surface were obtained by solution of the weak-collision master equation using Gillespie's exact stochastic simulation method,[42−44] explained in detail in our earlier paper[45] and discussed briefly here. In the energy-grained master equation, the ceiling energy considered was 200 kcal/mol above the initial :CHCHO adduct **Int1** and a small energy band size of 0.03 kcal/mol was chosen to ensure that the density of states does not change significantly within the band. To obtain the product distribution with high statistical precision, a large number of stochastic trials of ∼10^7 was used. In this application, the Mersenne Twister (MT19937)[46] random number generator was used.

The Lennard-Jones collision parameters for the bath gas He are $σ = 2.55$ Å and $ε/k_B = 10$ K.[47] Because no collision parameters for [C$_2$H$_2$O] are available in the literature, the values $σ = 4.08$ Å and $ε/k_B = 421$ K are estimated on the basis of

Kinetics Study of the O(^{3}P) + C$_2$H$_2$ Reaction

J. Phys. Chem. A, Vol. 110, No. 21, 2006 **6699**

Figure 1. Two lowest-lying triplet surfaces for the O(^{3}P) + C$_2$H$_2$ reaction constructed using the CBS-QCI/APNO (and CCSD(T)/6-311++G-(3df,2p)) levels of theory. The ^{3}A″ surface is shown by solid lines, whereas the ^{3}A′ surface is presented by dashed lines.

those of ethylene oxide C$_2$H$_4$O.[47] Thus, the collision frequency Z_{LJ} [M] was estimated at $\approx$1.1 × 10^{10} s^{-1} at 1 atm and room temperature. The probability density function for collision energy transfer was computed using the biexponential model of Troe.[48] An average energy transferred per collision $\langle\Delta E\rangle_{all}$ of -130 cm^{-1} was adopted. The initial energy distribution of formation of the triplet :CHCHO adduct **Int1** from O(^{3}P) + C$_2$H$_2$ via **TS1** was derived from detailed balance considerations.[49]

The statistical RRKM theory[49−54] of unimolecular reaction rates is used to compute the energy-specific rate constants $k(E)$ for a reactant with an internal energy E:

$$k(E) = \frac{\alpha}{h} \frac{G^\ddagger(E - E^\ddagger)}{\rho(E)} \qquad (3)$$

where α is the reaction pathway degeneracy, h is Planck's constant, $E^\ddagger$ is the barrier height for the reaction TS, $G^\ddagger(E-E^\ddagger)$ is the sum of vibrational states of the transition structure for energies from 0 up to $E - E^\ddagger$, and $\rho(E)$ is the density of states for a reactant molecule with internal energy E. The Beyer–Swinehart–Stein–Rabinovitch algorithm[55,56] was used to calculate the sum and density of states in eq 3 employing a grain size of 1 cm^{-1}.

As **TS6** in the **Int2**(:CHCHO) → **TS6** → H(^{2}S) + HCCO-(X^{2}A″) step is a loose transition structure (see next section), we used variational transition state theory[51−54] to locate the kinetic bottleneck. The CCSD(T)/6-311++G(d,p) and QCISD/6-311G(d,p) levels of theory were employed to optimize geometries and numerically calculate harmonic vibrational frequencies along the reaction coordinate (RC) using constrained optimizations for various fixed C−H bond lengths; energies along the RC were refined at the CCSD(T)/6-311++G-(3df,2p) and CBS-QCI/APNO levels of theory. Using this PES, $k(E)$ rate coefficients at every position along the RC were computed for internal chemical activation energies E of 54.4

(=49.1 + 5.3) or 53.9 (=50.4 + 3.5) kcal/mol (see Figure 1) and plotted in Figures S17 and S18 (see the Supporting Information), respectively. The minimal $k(E)$ was found for a C−H bond distance of 1.8 Å, and the characteristics at this point along the RC will be used in the subsequent kinetic calculations.

### III. Results and Discussion

III.1. Potential Energy Surfaces. Unless stated otherwise, the CCSD(T) results will be used for discussion in this section. The title reaction is initiated either by H-atom abstraction from acetylene by the oxygen atom or by electrophilic O-addition onto a C-atom in acetylene, following the spin conservation rule (see Figure 1). The H-abstraction channel proceeds through **TS2**, which is a very late, product-like transition structure with a long C−H bond distance of 1.567 Å and a short O−H bond of 1.031 Å (see Figure 3). Consequently, **TS2** lies very close to the products OH + HCC, 31.7 kcal/mol above the initial reactants as computed at the CBS-QB3 level. We were successful to locate **TS2** at the B3LYP and MP2 levels, but unsuccessful at the higher levels CCSD(T) and QCISD. Thus, the abstraction step appears to be barrierless. In any case, because of its high endothermicity of +31.9 kcal/mol, the H-abstraction channel cannot compete with the addition/elimination, below, under any combustion conditions.

Addition of the oxygen atom onto a C-atom in acetylene can take place on two different electronic state surfaces, ^{3}A″ and ^{3}A′, via **TS1** and **TS1-ex** leading to **Int1**(^{3}A″) and **Int1-ex**(^{3}A″), respectively. IRCMax(G2M:B3LYP)[57] calculations confirmed these connections (see Figure S7 in the Supporting Information), in which **TS1** (^{3}A″ state) lies 2.6 kcal/mol lower in energy than **TS1-ex** (^{3}A′ state). The C−O bond distances in these two transition structures are about 1.95 Å. We will now discuss the ^{3}A″ and ^{3}A′ surfaces individually.

^{3}A″ Electronic State Surface. **TS1** is a key kinetic reaction bottleneck and its barrier height and harmonic vibrational
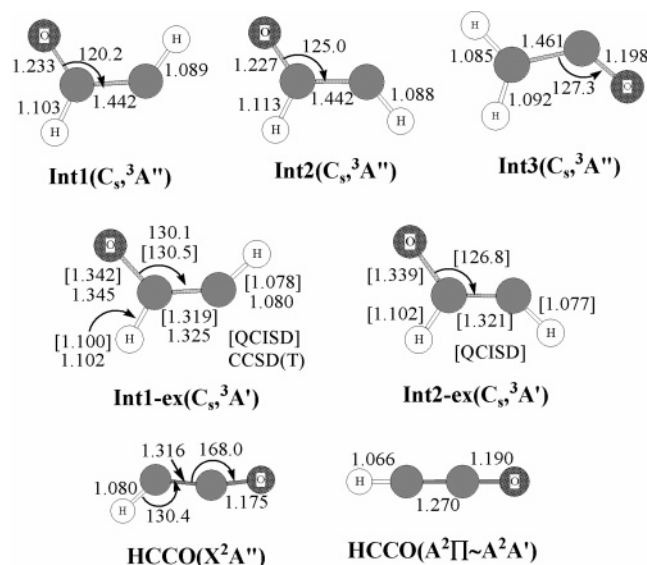
Figure 2. Optimized geometries obtained at the CCSD(T)/6-311++G-(d,p) level of theory, unless indicated otherwise, for some important minima in the O(^{3}P) + C$_2$H$_2$ reaction.
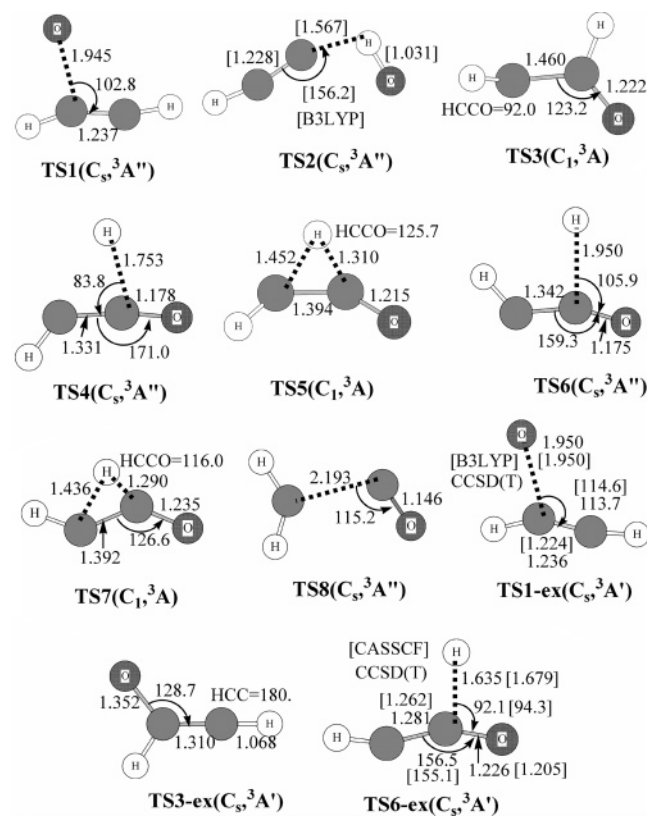
Figure 3. Optimized geometries obtained at the CCSD(T)/6-311++G-(d,p) level of theory, unless indicated otherwise, for transition structures in the O(^{3}P) + C$_2$H$_2$ reaction.

frequencies will be used for subsequent $k(T)$ TST calculations. To refine its computed characteristics, we carried out IRCMax-(CCSD(T)/6-311++G(3df,2p):CCSD(T)/6-311++G(d,p))[57] and IRCMax(CBS-QCI/APNO:QCISD/6-311G(d,p))[57] calculations (see Figure S8 in the Supporting Information) on this TS, yielding computed barrier heights of 5.3 and 3.5 kcal/mol at the CCSD(T) and CBS-QCI/APNO levels, respectively. The latter value is in good agreement with the experimental Arrhenius activation energy of 3–3.5 kcal/mol.[14,19,20]

Int1 is situated at 50.6 kcal/mol below the initial reactants. Both unpaired electrons are located on the C-atom with one orbital lying in-plane of the molecule and another out-of-plane (see two HOMOs of **Int1** in Figure S19 in the Supporting Information). As a result, the C=O distance of 1.233 Å in **Int1** is a double bond and the C–C of 1.442 Å is closer to a single bond. However, the two unpaired electrons on the radical carbon slightly delocalize along the C–C–O skeleton, resulting in additional stabilization of **Int1**. There are four possible reaction pathways from **Int1**, namely, (i) internal rotation over 180° about the C–C axis to form **Int2** via **TS3** with a low barrier height of 5.9 kcal/mol; (ii) 1,2-H migration to **Int3** through the a tight transition structure **TS5** with a barrier of 42.8 kcal/mol; (iii) H-elimination to form final products H(^{2}S) + HCCO(X^{2}A″) via **TS4** overcoming a barrier of 43.5 kcal/mol. **TS4** is somewhat looser than **TS5** and lies only 0.7 kcal/mol higher, such that the pathway via **TS4** appears more favorable than **TS5**; (iv) redissociation back to the initial reactants through **TS1** with a high barrier energy of 55.9 kcal/mol, which makes this step unimportant at any relevant temperature. It should be mentioned that **Int1** could do a 1,2-H shift from the central C-atom to the O-atom via **TS9** (not shown in Figure 1, see Figure S21 in the Supporting Information) leading to triplet HCCOH. However, this step faces a huge barrier of 64.6 kcal/mol computed at the CBS-QB3 level, so it is not relevant and will not be discussed further.

Int2 has an internal energy of 49.1 kcal/mol relative to the initial reactants. Its electronic structure is similar to that of **Int1**. Although **Int1** can be considered as a trans-configuration with the two H-atoms lying on opposite sides of the C–C bond, **Int2** has a cis-configuration. The trans ↔ cis isomerization is expected to occur rapidly in the chemically activated adducts because the internal rotation barrier is small, about 5–6 kcal/mol. A microcanonical **Int1** ↔ **Int2** preequilibrium may therefore be established. Note that **Int2** can only be produced from **Int1**, but not formed directly by addition of O to acetylene. Attempts to search a direct addition TS similar to **TS1** were unsuccessful; optimization always either converged back to **TS1** or failed to complete. As this issue is of importance (see below), to check the potential existence of this TS, we investigated the potential energy curve as a function of dihedral angle HCCO. Starting at the optimized geometry of **TS1** obtained at the CCSD(T)/cc-pVTZ level with HCCO = 0°, we increased the HCCO angle up to 180° in steps of 10°. At every new position, a single-point calculation was done at the same CCSD(T) level. The computed results, plotted in Figure 4, show that the cis-configuration TS is a second-order saddle point, smoothly connected to **TS1** on either side. Therefore, a first-order minimum energy pathway connecting the initial reactants directly to **Int2** is not expected to exist.

Int2 can eliminate the H-atom at the center carbon atom forming the products H(^{2}S) + HCCO(X^{2}A″). This channel proceeds via **TS6** and faces a barrier height of 34.3 kcal/mol. **TS6** is a very loose saddle point structure with C–H bond distance r(C–H) = 1.95 Å. We used variational transition state theory to locate the rate-limiting bottleneck. This kinetic bottleneck structure is somewhat tighter with r(C–H) = 1.8 Å, i.e., 0.15 Å shorter than in the saddle point **TS6**. **Int2** isomerizes by a 1,2-H migration via **TS7**, a tight TS, leading to triplet ketene (**Int3**) after clearing a barrier of 49.4 kcal/mol.

Triplet ketene (**Int3**) as formed from **Int1** and **Int2** possesses a high internal energy of 69.2 kcal/mol. Hence, it is predicted to decompose rapidly into fragments CH$_2$(X^{3}B$_1$) + CO via the low-lying **TS8**. This channel faces a barrier of 25.3 kcal/mol,
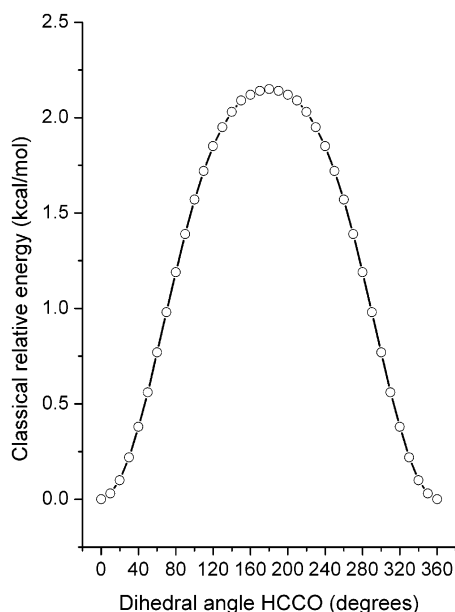
Figure 4. Potential energy curve as a function of the dihedral angle HCCO in **TS1** computed at the CCSD(T)/cc-pVTZ level of theory.

about 36 kcal/mol lower than for isomerization back to **Int1** or **Int2**. Therefore, reisomerization is very unlikely.

In summary, calculations for the ^{3}A″ state presented in Figure 1 show that initial O-addition to acetylene leads entirely to vibrationally excited adduct **Int1**, which could quickly set up a microcanonical preequilibrium with its rotamer **Int2**. This near-equilibrium system either can lose a H-atom forming final products H(^{2}S) + HCCO(X^{2}A″) or can proceed further by a 1,2-H shift leading to triplet ketene, followed by fast dissociation into final products CH$_2$(X^{3}B$_1$) + CO. Because **TS5** and **TS7** for H-migration are tighter and lie higher in energy than **TS4** and **TS6** for H-elimination, the steps via the latter transition structures are more favorable than the former. Consequently, the H(^{2}S) + HCCO(X^{2}A″) products yield is theoretically expected to dominate the CH$_2$(X^{3}B$_1$) + CO yield, in accord with experiment.[7−9]

It should be mentioned that in their theoretical studies, Gigard and Chaquin[23] reported the ring structures that could result from C$_2$H$_2$ + O(^{3}P) to lie very high in energy on the triplet surface, such that they are not expected to play any role in the reaction.

^{3}A′ Electronic State Surface. Electrophilic addition of oxygen atom onto a C-atom in acetylene can also proceed on the ^{3}A′ state surface via **TS1-ex** leading to **Int1-ex**. This step needs to overcome a barrier of 6.1 kcal/mol. **TS1-ex** was found to be a first-order saddle point at the B3LYP, MP2, and CASSCF levels of theory, but a second-order saddle point with two imaginary wavenumbers at the CCSD(T) and QCISD levels. Hence, the true **TS1-ex** saddle point may in reality belong to the C_1 symmetry point group rather than C_s, thus resulting in a slight reduction in its energy which should increase the predicted overall thermal rate coefficient. This is important at high temperatures, where theoretical calculations remain underestimates compared to experiment[7,14] (see also below).

Int1-ex has an internal energy of 21.0 kcal/mol relative to the initial reactants. **Int1-ex** is a biradical featuring two unpaired electrons, both of which move in the molecular plane. One is located on the O-atom, the other on the C-atom (see its two HOMOs in Figure S19 in the Supporting Information). Consequently, the C=C distance of 1.325 Å is close to a double bond, whereas the r(C−O) of 1.345 Å is between a single and double bond (see Figure 2). The apparent slight delocalization

of the unpaired electron of the O-atom along the C−C−O skeleton should provide some additional stabilization. There is another conformer of **Int1-ex**, that is **Int2-ex**, which has a cis-form and lies 0.7 kcal/mol lower. Fast preequilibration of the **Int1-ex** and **Int2-ex** isomers is expected as this step, via **TS3-ex**, faces a barrier of only ∼1−2 kcal/mol. Note that the configuration change from trans- to cis-form in this case proceeds by bending the HCC angle in the molecular plane, unlike the ^{3}A″ **Int1** ↔ **Int2** isomerization that occurs by internal rotation. The HCC angle in **TS3-ex** is exactly equal to 180° (see Figure 3). Note that no TS could be found that directly connects the reactants to **Int2-ex**; moreover, the energy of **TS1-ex**-like ^{3}A′ structures as a function of the HCC angle was found to show only a single minimum, at ≈170°, i.e., the **TS1-ex** geometry (see Figure 2). This is not inconsistent with the "excited" entrance transition state actually being of C_1 symmetry.

Int2-ex can lose a H-atom at the center C-atom leading to electronically excited products H(^{2}S) + HCCO(A^{2}A′), about ∼3 kcal/mol above the ground-state products H(^{2}S) + HCCO-(X^{2}A″). This step proceeds through **TS6-ex** and faces a barrier height of 18.2 kcal/mol. **TS6-ex** is a first-order saddle point at the CASSCF and B3LYP levels (see IRC analysis, the Supporting Information), but a second-order saddle at the QCISD and CCSD(T) levels. Again, this indicates that the true **TS6-ex** saddle point may have a C_1 symmetry, such that the barrier of this step is even lower and more favorable for decomposition of **Int2-ex**.

Int1-ex could also redissociate back to the initial reactants via **TS1-ex** with a barrier height of 28.6 kcal/mol. However, **TS1-ex** is tighter and is ∼11 kcal/mol higher than **TS6-ex**, indicating that redissociation is disfavored. Finally, internal conversion of **Int1-ex** to the lowest-lying triplet, **Int1** is very unlikely because the lifetime of **Int1-ex** is estimated to be only ∼1 ps. Hence, **Int-ex** is expected to almost entirely fragment into the electronically excited products H(^{2}S) + HCCO(A^{2}A′), thus increasing the H and HCCO products yield. This product-forming pathway through the ^{3}A′ state—newly identified as far as we are aware—should be especially important at high temperatures. Note that in their investigation, Harding and Wagner[14] found no correlation of the excited initial ^{3}A′ adduct with an accessible products state and so concluded that it should preferentially redissociate back into the initial reactants, at least at temperatures > 1000 K. The (two-step) connection identified presently: **Int1-ex** → **TS3-ex** → **Int2-ex** → **TS6-ex** → H(^{2}S) + HCCO(A^{2}A′) is fully supported by IRC-analyses (see the Supporting Information).

It is of interest to evaluate the relative importance of the routes on the ^{3}A′ and ^{3}A″ surfaces. The ratio of the two rate coefficients is given by the relative thermal population of the two entrance-channel transition states **TS1** and **TS1-ex**, and therefore by their partition function ratio. Thus, the fractional contribution of the **TS1-ex** route can be expressed as

$$P_{ex} = \frac{Q_{TS1-ex} \exp(-E_{TS1-ex}/RT)}{Q_{TS1-ex} \exp(-E_{TS1-ex}/RT) + Q_{TS1} \exp(-E_{TS1}/RT)} \quad (4)$$

The results plotted in Figure 5 show that P_{ex} depends strongly on temperatures; P_{ex} rises from a low ∼1% at 300 K to ∼30% at T = 2000 K, indicating that the reaction on the ^{3}A′ surface yielding H(^{2}S) + HCCO(A^{2}A′) contributes substantially in flames.
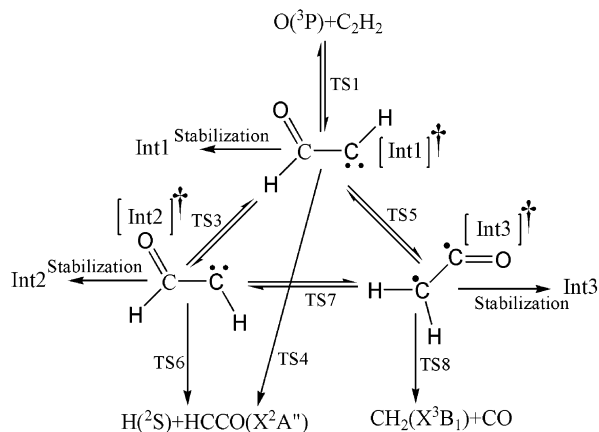
III.2. Overall Primary Product Distribution. *Temperature and Pressure Dependence.* Based on the triplet ^{3}A″ electronic

6702 *J. Phys. Chem. A, Vol. 110, No. 21, 2006*

Nguyen et al.
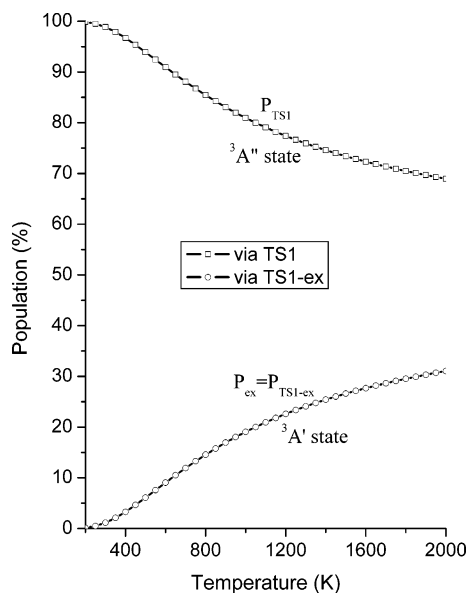
Figure 5. Fractional populations of the **TS1-ex** and **TS1** transition states for the initial addition steps as a function of temperature.

SCHEME 1

TABLE 3: Computed Products Distribution (%) at 1 Atm as a Function of Temperature for the O(^{3}P) + C$_2$H$_2$ Reaction Occurring on the ^{3}A″ State Surface Using Kinetic Scheme 1

T (K)	H(^{2}S) + HCCO(X^{2}A″)	CH$_2$(X^{3}B$_1$) + CO	O(^{3}P) + C$_2$H$_2$	OC$_2$H$_2$
298	93.1[a]	6.9	0.0	0.0
	(92.1)[b]	(7.9)	(0.0)	(0.0)
500	92.4	7.5	0.1	0.0
	(91.4)	(8.5)	(0.1)	(0.0)
800	91.1	8.6	0.3	0.0
	(90.3)	(9.5)	(0.2)	(0.0)
1000	90.2	9.3	0.5	0.0
	(89.5)	(10.1)	(0.4)	(0.0)

[a] Using the CCSD(T)/6-311++G(3df,2p) PES with ZPE from unscaled CCSD(T)/6-311++G(d,p) harmonic vibrational frequencies. [b] Using the CBS-QCI/APNO PES with ZPE from QCISD/6-311G(d,p) harmonic vibrational frequencies scaled down by 0.9538.[69]

state surface in Figure 1, a reduced reaction scheme for kinetic calculations is presented in Scheme 1.

First, we carried out product distribution calculations for the ^{3}A″ pathways by solving the master equation under reaction conditions $T = 298-1000$ K and $P \leq 1$ atm, where the available experimental data shows a HCCO + H yield ≈80% and CH$_2$-(X^{3}B$_1$) + CO yield ≈20%, independent of temperature. Our results based on the CCSD(T) and CBS-QCI/APNO data agree well with each other (see Table 3). The difference between the two approaches is negligible (~1%), indicating that the computed product distribution is not sensitive to the quantum chemical methodology used in this work. In the discussion below we will refer to the CCSD(T) results.

Table 3 shows that the computed product distribution is slightly dependent on temperature. The H(^{2}S) + HCCO(X^{2}A″) yield is 93% at 300 K and drops to 90% at 1000 K, whereas the CH$_2$(X^{3}B$_1$) + CO yield rises from 7% at 300 K to 10% at 1000 K. It should be noted that about 82% of the products at 300 K thus computed result directly from **Int2** and only 18% from **Int1**; this is mainly due to the ~7.0 kcal/mol lower TS from **Int2** for forming the major products, H + HCCO (see **TS6** versus **TS4** in Figure 1) and the very high **Int1 ↔ Int2** interconversion rates as given by conventional RRKM.

We examined the possible impact of H-atom tunneling, using the asymmetrical Eckart potential,[58] but the effects were found to be unimportant. For example, at $T = 298$ K tunneling treatments increase the absolute yield of triplet CH$_2$ by only 0.6%, from 6.9% to 7.5%, whereas at $T = 1000$ K the increase of the triplet CH$_2$ yield is only 0.4%. This small impact of tunneling is expected, as the adducts have chemical-activation internal energies that are much higher than the barriers of the decomposition channels.

Thus, our computed CH$_2$(X^{3}B$_1$) + CO yield, of 7−10%, is about twice smaller than the experimental data (15%[8,9] to ~20%[7]); it will be reduced even further when the ^{3}A′ reaction path is taken into account for $T > 1000$ K.

To find other possible source(s) of the discrepancy, we investigated the sensitivity of the quantum chemical results to the basis set size, which could influence the PES and hence the product branching ratios. As can be seen in Figure 1, the products CH$_2$(X^{3}B$_1$) + CO formed from activated triplet ketene are kinetically controlled by **TS5** and **TS7**, whereas the products H(^{2}S) + HCCO(X^{2}A″) are formed through **TS4** and **TS6**. Further CCSD(T) calculations with larger basis sets for optimization and energy, tabulated in Table 2, show that relative energies for these transition states are not sensitive to the basis sets used, within ~0.5 kcal/mol, such that the basis sets are unlikely to influence the predicted product distribution beyond ~2%. Likewise, the calculations at other high levels of theory (vide infra) agree very well with our CCSD(T) data.

Note that the estimated worst-case CCSD(T) relative-energy error is about 2 kcal/mol. Shifting up the position of **TS6** by 2.0 kcal/mol results in a 3% increase of the absolute CH$_2$(X^{3}B$_1$) + CO yield at $T = 298$ K, to 10%, i.e., still approximately 2 times smaller than the experimental yield of 20%. To reproduce the latter, **TS6** would have to be shifted up by 6 kcal/mol, i.e., to the same position as **TS4**. Such large CCSD(T) relative-energy errors on very similar structures are extremely unlikely.

Hence, even when other accurate quantum chemical levels of theory were to be used, the change required in relative energies or transition state tightness to match the experimental data is significantly larger than the margins of uncertainty on our quantum chemical data. Rather, the systematic underestimation of the computed product distribution seems to imply that the branching ratios of the O(^{3}P) + C$_2$H$_2$ reaction on the ^{3}A″ surfaces behave nonstatistically, i.e., that the statistical RRKM theory fails for certain intermediate steps.

We now attempt to explain this suspected nonstatistical behavior of the O(^{3}P) + C$_2$H$_2$ reaction. The product distribution computed above actually implies fast **Int1 ↔ Int2** interconversion rates $>10^{13}$ s^{-1} as given by the standard RRKM

Kinetics Study of the O(^{3}P) + C$_2$H$_2$ Reaction

J. Phys. Chem. A, Vol. 110, No. 21, 2006 **6703**

TABLE 4: Computed Products Distribution (%)^a as a Function of Temperature at $P = 1$ Atm for the O(^{3}P) + C$_2$H$_2$ Reaction Occurring on the ^{3}A″ Electronic State Surface Using Reaction Kinetic Scheme 1 and Allowing for Nonstatistical Behavior of Internal Rotation in Int1^b

T (K)	H + HCCO(X^{2}A″)	CH$_2$(X^{3}B$_1$) + CO	O(^{3}P) + C$_2$H$_2$	OC$_2$H$_2$
298	79.0	20.9	0.1	0.0
500	77.3	22.4	0.3	0.0
800	75.2	24.0	0.8	0.0
1000	74.1	24.6	1.3	0.0
1200	73.3	24.9	1.8	0.0
1500	72.2	25.0	2.8	0.0
1800	71.5	24.7	3.8	0.0
2000	71.0	24.5	4.5	0.0

^{a} Using the CCSD(T)/6-311++G(3df,2p) PES with ZPE from unscaled CCSD(T)/6-311++G(d,p) harmonic vibrational frequencies. ^{b} Effective total internal energy of **Int1** available for statistical partitioning into the internal rotation mode scaled down by a factor 0.4 (see text).

formalism, and therefore a microcanonical near-equilibrium **Int1/Int2** ratio close to unity at the high total internal energies of ≈55 kcal/mol involved. As compared to **Int1**, the rotamer **Int2** faces a much lower barrier for H-atom elimination but a higher one for isomerization to triplet ketene (see Figure 1), such that the reaction flux through **Int2** is high and leads almost solely to H(^{2}S) + HCCO(X^{2}A″) and almost no CH$_2$(X^{3}B$_1$) + CO. Thus, the fast **Int1** ↔ **Int2** conversion implied by RRKM increases the deviation of the computed product distribution from the experiment. However, the conventional RRKM formalism assumes that the total internal energy of **Int1** is *statistically* distributed over all internal modes, including the torsional vibration corresponding to hindered internal rotation about the C−C axis, which governs the **Int1** ↔**Int2** isomerization. If this mode were to remain underactivated, the experimental product branching ratio could easily be explained. Such a *sub*statistical energy partitioning would greatly slow **Int1** → **Int2** isomerization, allowing for a larger fraction of the products being formed from **Int1** and hence increasing the yield of CH$_2$(X^{3}B$_1$) + CO. Dynamic (trajectory) calculations are required to validate this assumption but are far beyond the scope of this study. Nonetheless, for the case at hand such a nonergodic behavior cannot be dismissed off-hand. For any approach of the oxygen, any out-of-plane excitation would involve torsional effects on the hydrogens. These atoms, however, are light and furthermore located very close to the axis of the acetylene molecule even at distances where the presence of the oxygen atom already distorts the axial acetylene symmetry. Both these factors result in a very low relative moment of inertia, such that any out-of-plane impulse imparted by the O-atom is channeled toward overall molecular rather than internal rotation. Hence, we propose that the rate of internal-rotation isomerization is hampered by nonstatistical energy partitioning in the initial adduct. To reproduce the experimental product branching ratios in the frame of this assumption, the specific **Int1** ↔ **Int2** interconversion rates, as obtained from eq 3, are reduced by scaling down the *effective* total internal energy (E) that is available for *statistical* partitioning into the torsional mode of interest. An effective-energy scaling factor of 0.4 matches the experimentally observed product distribution at 300 K. An efficiency factor of this magnitude appears reasonable for the case at hand, and we will adopt it over the entire energy range. The computed results are presented in Table 4. Note that the energy scaling factor of 0.4 for the torsion mode entails that the **Int1** ↔ **Int2** isomerization rates, relative to the product

formation rates, decrease by a factor 200 over the short (≈10 ps) lifetime of the initial **Int1** adduct. Yet, the steady-state population ratio **Int2/Int1** decreases much less, by a factor of 6.3; the fraction of products resulting directly from **Int1** increases to 58% (instead of 18%), whereas the contribution from **Int2** decreases to 42% (instead of 82%).

It should be noted that treating the internal rotation mode in **Int1** (or **Int2**) as a hindered rotor instead of a harmonic oscillation should lower the statistical RRKM-calculated rates of the **Int1** ↔ **Int2** isomerization. However, this decrease would be at most a factor of ≈4, whereas the experimental CH$_2$/HCCO branching ratio requires ≈200 times lower rates than the conventional RRKM harmonic oscillator approximation. Such a limited reduction of these large rates would leave the steady-state population ratio **Int2/Int1** almost unchanged—i.e., still close to the microcanonical preequilibrium—and hence can shift the predicted absolute product yields by at most 1%.

In a similar vein, one should also consider possible anharmonicity effects influencing the rates of critical reaction steps to rationalize the discrepancy above. The potentially most sensitive reaction in this respect is **Int2** → H(^{2}S) + HCCO-(X^{2}A″) via **TS6**, which carries 80% of the reaction flux in the conventional harmonic oscillator RRKM approximation—the more so as **TS6** is the most loose of all transition structures involved here and therefore appears most susceptible to vibration anharmonicities. However, the magnitudes of the vibration frequencies of both **TS6** and **Int2** (see Supporting Information) are not suggestive of important anharmonic effects. Moreover, a detailed analysis shows that the rate of the **Int2** → H(^{2}S) + HCCO(X^{2}A″) step should be a factor of 6 lower than the statistical RRKM value to match the measured CH$_2$ and HCCO yields at room temperature. Clearly, such a large anharmonicity effect appears highly unlikely.

Another possible alternative rationalization for the too low predicted CH$_2$ yield that needs to be examined, is that triplet HCCHO (**Int1** or **Int2**) might also undergo competitive intersystem crossing (ISC) to singlet HCCHO, which should rapidly isomerize to the low-lying singlet ketene H$_2$C=CO and so yield singlet CH$_2$(^{1}A$_1$) + CO. A ca. 10% primary CH$_2$(^{1}A$_1$) yield by this hypothetical route would explain the discrepancy between theory and experiment, above. It must be noted that small amounts of singlet CH$_2$(^{1}A$_1$) have been observed in C$_2$H$_2$/O/H "atomic flame" systems, in this laboratory, by laser-induced fluorescence and as well as molecular-beam mass spectrometry techniques; however, the large body of evidence gathered on its formation route consistently demonstrates it to be a secondary product from the fast HCCO + H reaction, while ruling out any significant primary production by the C$_2$H$_2$ + O reaction.[6,8,9,59] The absence of significant triplet → singlet ISC in this reaction—though important ISC was recently confirmed by us in both the C$_2$H$_4$ + O(^{3}P) and C$_2$F$_4$ + O(^{3}P) reactions[60,61]—can be attributed to (i) the faster chemical decomposition of the chemically activated triplet HCCHO adduct **Int1** and (ii) a slower ISC on account of the HCCHO triplet and singlet surface crossing seams being restricted to a narrower geometry range. Indeed, as shown in Figure S22 of the Supporting Information, at the CBS-QB3 level of theory, the lowest singlet HCCHO (^{1}A state, point group C_1) was found to lie 4 kcal/mol above **Int1**(^{3}A″), featuring a sharp minimum for a 90° HCCO dihedral angle, just touching the triplet surface at the **TS3** saddle point for the internal rotation of **Int1**(^{3}A″) to **Int2**(^{3}A″). Thus, the negligible ISC that follows from the cited experimental evidence is fully consistent with the substatistical activation of the internal rotation mode in **Int1** as put forward above.

TABLE 5: Computed Overall Products Distribution (%)[a,b] for the O(^{3}P) + C$_2$H$_2$ Reaction at 1 Atm as a Function of Temperature

T (K)	H(^{2}S) + HCCO(X^{2}A″+A^{2}A′)[c]	CH$_2$(X^{3}B$_1$) + CO	O(^{3}P) + C$_2$H$_2$	OC$_2$H$_2$
298	79.2 (78.1 + 1.1)	20.7	0.1	0.0
500	78.7 (72.6 + 6.1)	21.1	0.2	0.0
800	78.9 (64.3 + 14.6)	20.5	0.6	0.0
1000	79.1 (60.0 + 19.1)	19.9	1.0	0.0
1200	79.3 (56.7 + 22.6)	19.3	1.4	0.0
1500	79.6 (53.0 + 26.6)	18.3	2.1	0.0
1800	79.9 (50.4 + 29.5)	17.4	2.7	0.0
2000	80.0 (49.0 + 31.0)	16.9	3.1	0.0

[a] Using the CCSD(T)/6-311++G(3df,2p) PES with ZPE from unscaled CCSD(T)/6-311++G(d,p) harmonic vibrational frequencies. [b] Effective total internal energy of **Int1** available for statistical partitioning into the internal rotation mode scaled down by a factor 0.4 (see text). [c] The first and second values in parentheses give the H + HCCO contributions from the reactions on the ^{3}A″ and ^{3}A′ surfaces, respectively.

Therefore, it appears that the nonergodic behavior argued above offers the only viable explanation for the observed product distribution. The product distribution so obtained above for the ^{3}A″ surface, is then combined with the branching ratio for the initial addition of the O-atom with acetylene via the ^{3}A″ and ^{3}A′ states, to derive the overall primary product distribution as a function of temperature, whereby it should be noted again that the reaction on the excited ^{3}A′ triplet surface becomes important only at higher temperatures. The resulting product distribution data, presented in Table 5, shows that the total H(^{2}S) + HCCO yield is ~80%, nearly independent of temperature over the wide range 298−2000 K, whereas the yield of CH$_2$-(X^{3}B$_1$) + CO weakly decreases from ~21% at 298 K to ~17% at 2000 K, in good agreement with the experimental yields for T = 290−1200 K. However, it should be emphasized that the constancy of the computed yields with increasing temperature is largely owed to the strongly increasing contribution of the reaction on the ^{3}A′ surface, which produces only H(^{2}S) + HCCO(A^{2}A′) (see Table 5). The fraction of redissociation of initial adducts back to the reactants is minor (< 5%), whereas there is no stabilization of triplet intermediates at atmospheric pressures and below. This last result is easily understood given that the transition states for decomposition of the triplet adduct lie much lower in energy than the addition transition structures of the first reaction step. The lifetime of triplet adduct HCCHO **Int1** is estimated to be ~15 ps at T =1000 K and reduces to ~4 ps at T = 2000 K. Moreover, it requires dozens of collisions to stabilize this vibrationally excited adduct below the energy level of the lowest-lying decomposition TS. It can therefore be predicted that the product distribution does not depend significantly on pressure for practical combustion systems.

Collision-Free Conditions. Finally, it is of interest to compare our computed primary product distribution with that recently observed in the collision-free, energy-specific molecular beam study by Casavecchia and co-workers.[11] This experiment was carried out at a collision energy of 9.5 kcal/mol. We assume here that this is converted entirely to additional internal vibration energy of the initially formed triplet adduct : CHCHO. Note that a similar average thermal energy of the reactants is acquired at a temperature of about 750 K. Microcanonical rate constants for various channels in the O(^{3}P) + C$_2$H$_2$ reaction computed at an internal energy of 9.5 kcal/mol above the initial reactants are displayed in Table 6. As can be seen, the value of k_6 is ~7 × 10^{13} s^{-1}, which is much faster than the rate of internal energy redistribution (10^{12}−10^{13} s^{-1}). Hence, non-RRKM behavior is

TABLE 6: Calculated Microcanonical Rate Constants (s^{-1}) for the Various Steps in the O(^{3}P) + C$_2$H$_2$ Reaction Occurring on the ^{3}A″ Electronic State Surface under Collision-Free Conditions in the Molecular Beam Experiment with an Initial Collision Energy of 9.5 kcal/mol[a]

reaction step	k(E) (s^{-1})
Int1 → TS3 → Int2	$k_1 = 2.13 \times 10^{10}$ [a]
Int2 → TS3 → Int1	$k_{-1} = 5.10 \times 10^{10}$ [a]
Int1 → TS5 → Int3	$k_2 = 1.68 \times 10^{10}$
Int3 → TS5 → Int1	$k_{-2} = 4.84 \times 10^{9}$
Int2 → TS7 → Int3	$k_3 = 2.68 \times 10^{9}$
Int3 → TS7 → Int2	$k_{-3} = 3.24 \times 10^{8}$
Int1 → TS4 → H + HCCO(X^{2}A″)	$k_4 = 3.52 \times 10^{10}$
Int2 → TS6 → H + HCCO(X^{2}A″)	$k_5 = 4.21 \times 10^{11}$
Int3 → TS8 → CH$_2$(X^{3}B$_1$) + CO	$k_6 = 7.04 \times 10^{13}$

[a] Effective total internal energy of **Int1** available for statistical partitioning into the internal rotation mode scaled down by a factor 0.4 (see text).

expected as the statistical energy partitioning assumption breaks down. However, in this case the very large value for k_6 simply implies that all the activated triplet ketene, once formed, immediately decomposes to products CH$_2$(X^{3}B$_1$) + CO. Similar to calculations for the thermal reaction above, we also scaled down the effective total internal energy that is available for *statistical* partitioning into the torsional mode by a factor of 0.4. Solving the master equation for the reaction on the ^{3}A″ surface yields 76% H(^{2}S) + HCCO(X^{2}A″) and 24% CH$_2$(X^{3}B$_1$) + CO.

To compute the overall primary product distribution, the relative contributions of the initial addition steps need to be known at a collision energy of 9.5 kcal/mol. This ratio can be evaluated if the reaction cross section for the reaction of the O-atom with acetylene is available. According to Marcus,[62,63] Morokuma,[64] and Lin,[65] an average reaction cross section at an internal energy E for a bimolecular reaction is expressed as follows:

$$\langle \sigma(E) \rangle = \frac{\kappa h^2}{8\pi\mu} \frac{G^{\ddagger}(E - E^{\ddagger})}{\epsilon(E)} \quad (5)$$

where κ is the transmission coefficient, μ is the reduced mass, $G^{\ddagger}$ is the sum of states for the addition transition structure, and ϵ is the energy density function for the initial reactants, which is given as

$$\epsilon(E) = \frac{1}{2\pi i} \int_{\gamma - i\infty}^{\gamma + i\infty} \frac{Q_{int}(\beta)}{\beta^2} e^{\beta E} d\beta \quad (6)$$

with $\beta = 1/k_b T$, and Q_{int} the internal partition function for the reactants.

Using eq 6, a branching ratio (BR) at an internal energy E for the ^{3}A′ and ^{3}A″ reaction channels can be computed as the ratio of the sum of states for **TS1-ex** and the sum of states for **TS1**.

$$BR(E) = \frac{G^{\ddagger}(E - E^{\ddagger}_{TS1-ex})}{G^{\ddagger}(E - E^{\ddagger}_{TS1})} \quad (7)$$

At a collision energy ($E_c = E$) of 9.5 kcal/mol, BR is computed to be ~0.19, thus resulting in a population of 16% for the ^{3}A′ state and of 84% for the ^{3}A″ state. Finally, combining these values with the product branching ratios on the ^{3}A″ and ^{3}A′ state, the overall primary product distribution predicted for E_c = 9.5 kcal/mol is derived as 80% (79% ± 5%) for H + HCCO and 20% (21% ± 5%) for CH$_2$(X^{3}B$_1$) + CO, with the

Kinetics Study of the O(^{3}P) + C$_2$H$_2$ Reaction

J. Phys. Chem. A, Vol. 110, No. 21, 2006 **6705**

experimental data given in parentheses for the purpose of comparison. Again, our computed yields agree well with those observed experimentally.

III.3. Overall Thermal Rate Coefficient. The overall temperature-dependent rate coefficient $k(T)_{\text{overall}}$ for the O(^{3}P) + C$_2$H$_2$ reaction can be computed according to the following expression:

$$k(T)_{\text{overall}} = (1 - \gamma_{\text{re}})k_{\text{TST}}(T) \qquad (8)$$

where γ_{re} is the fraction of redissociation of the initial adducts back to the initial reactants, O(^{3}P) + C$_2$H$_2$. The value of γ_{re} is a function of pressure and temperature (see Table 5). $k_{\text{TST}}(T)$ is the rate coefficient derived from multistate transition state theory:

$$k(T)_{\text{TST}} = \frac{k_{\text{b}}T}{h} \frac{Q^{\ddagger}_{\text{TS1}}\exp(-E^{\ddagger}_{\text{TS1}}/RT) + Q^{\ddagger}_{\text{TS1-ex}}\exp(-E^{\ddagger}_{\text{TS1-ex}}/RT)}{Q_{\text{O}}Q_{\text{C}_2\text{H}_2}} \qquad (9)$$

where $Q(T)$ is a complete partition function, k_{b} is Boltzmann's constant, h is Planck's constant, R is the universal gas constant, and $E^{\ddagger}_{\text{TS1}}$ and $E^{\ddagger}_{\text{TS1-ex}}$ are the barrier heights, of 3.0 and 5.6 kcal/mol used (see explanation below) for the initial addition steps on the ^{3}A″ and ^{3}A′ surfaces, respectively. The rotational symmetries for C$_2$H$_2$ and the transition states are 2 and 1, respectively, such that the reaction path degeneracy is 2. The electronic partition function of the O atom explicitly includes the three lowest-lying electronic states (^{3}P$_2$ with electronic degeneracy $g = 5$, ^{3}P$_1$ with $g = 3$, and ^{3}P$_0$ with $g = 1$), with relative energies of 0.0000, 0.4525, and 0.6490 kcal/mol, respectively.[66] In addition, the electronic degeneracy of 3 for **TS1** and **TS1-ex**, both having a triplet electronic state, is also taken into account.

Although our computed CBS-QCI/APNO barrier height of 3.5 kcal/mol for **TS1** is in agreement with the experimental Arrhenius activation energy (3–3.5 kcal/mol),[7,19,20] the value of $k(T)$ computed at room temperature using this barrier height is 6×10^{-14} cm^3 molecule^{-1} s^{-1}, ∼2.3 times smaller than that observed in experiments: 1.4×10^{-13} cm^3 molecule^{-1} s^{-1}.[21] Therefore, we estimated the relative energy of **TS1** in an alternative way by forcing $k(T)$ computed using eq 8 to match the experimental k at 300 K, but while keeping the energy difference between **TS1** and **TS1-ex** at 2.6 kcal/mol. In this way, a relative energy of 3.0 kcal/mol was obtained for **TS1**, and hence 5.6 kcal/mol for **TS1-ex**. Using these barrier heights, both 0.5 kcal/mol below the CBS-QCI/APNO values, we computed overall thermal rate coefficients for the wide temperature range 200–2000 K; they can be summarized by the modified-Arrhenius expression $k(T) = 6.14 \times 10^{-15}T^{1.28}\exp(-1244\ \text{K}/T)$ cm^3 molecule^{-1} s^{-1}.

The rate predictions are plotted in Figure 6, together with the more recent experimental data for comparison. Our $k(T)$ results are in near-perfect agreement with the experimental values obtained since 1990 over the entire range 200–2000 K, spanning over 3 orders of magnitude. This excellent agreement is due to a large extent to the newly characterized reaction pathway on the excited ^{3}A′ surface, which carries ca. 30% of the reaction flux at 2000 K.

IV. Conclusions

In the present theoretical study, the two lowest-lying triplet potential energy surfaces for the O(^{3}P) + C$_2$H$_2$ reaction are constructed, uniformly using high levels of theory such as
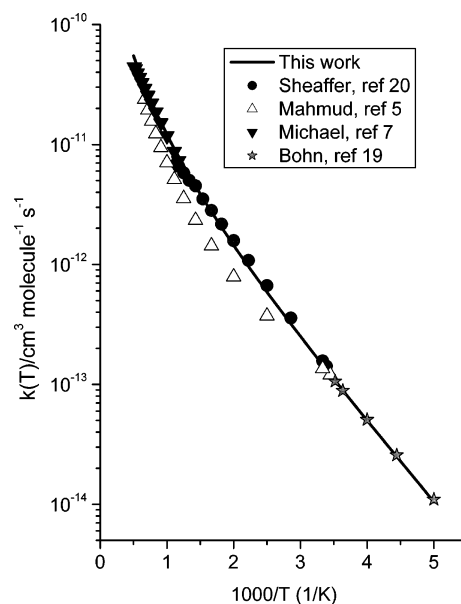
Figure 6. Overall thermal rate coefficients computed at temperatures in the range of 200–2000 K. Experimental data are given for the purpose of comparison.

CCSD(T) and CBS-QCI/APNO. RRKM-master equation calculations to evaluate primary product distribution were carried out using the exact stochastic simulation method. In addition, overall thermal rate coefficients were determined using conventional transition state theory. A number of important results emerge from this study and can be summarized as follows:

(i) The O(^{3}P) + C$_2$H$_2$ reaction is confirmed to occur near-exclusively via an electrophilic addition mechanism as the first reaction step.

(ii) The levels of theory used in our quantum chemical calculations yield results in better agreement with available experimental data compared to previous theoretical results.

(iii) The newly characterized reaction path on the ^{3}A′ surface results in electronically excited products H(^{2}S) + HCCO(A^{2}A′) and is predicted to be important at high temperatures. Its contribution to overall product formation is estimated to be ca. 30% at 2000 K.

(iv) Conventional-RRKM product yields depart from the experimental branching fractions by some 10 percentage points, suggesting a nonstatistical energy distribution in the chemically activated initial adduct *trans*-**Int1** that reduces its rate of internal-rotation to form *cis*-**Int2**. When the **Int1** ↔ **Int2** rates are scaled down so as to match the experimental product branching at 300 K, the computed product yields agree well with those observed over the entire experimental 290–1200 K region. It should be noted, however, that the predicted near-constancy of the product yields over the wide 200–2000 K range, ∼80% H(^{2}S) + HCCO and ∼20% CH$_2$(X^{3}B$_1$) + CO, is due to a large extent to the pathway on the excited surface, ^{3}A′.

(v) Using the same scaling factor for the **Int1** ↔ **Int2** isomerization as above, the product distribution evaluated for collision-free conditions is in good agreement with recent molecular beam measurements at a collision energy of 9.5 kcal/mol.[11]

(vi) Reducing the CBS-QCI/APNO computed entrance channel barriers by 0.5 kcal/mol so as to fit the experimental data at 300 K, the computed overall TST rate coefficient for the range 200–2000 K: $k(T) = 6.14 \times 10^{-15}T^{1.28}\exp(-1244\ \text{K}/T)$ cm^3 molecule^{-1} s^{-1}, is in excellent agreement with the experimental data over the entire range. The newly characterized reaction

path on the excited $^3A'$ surface accounts quantitatively for the too low earlier theoretical $k(T)$ predictions at the higher temperatures.[7,14]

(vii) Of the ab initio methods applied here, CBS-QCI/APNO affords the best match of the experimental energies for the radical products as well as the entrance transition states.

Supporting Information Available: Optimized geometries, zero-point energies, total energies, relative energies, rotational constants, harmonic vibrational frequencies, IRC calculations, and the most important configuration coefficients in a wave function are listed in the Supporting Information. In addition, numerous graphs are presented on the IRC calculations and the orbitals of key components. This material is available free of charge via the Internet at http://pubs.acs.org.

References and Notes

(1) Williams, A.; Smith, D. B. *Chem. Rev.* **1970**, *70*, 267.

(2) Peeters, J. *Bull. Soc. Chim. Belg.* **1997**, *106*, 337 and references therein.

(3) Peeters, J.; Schaekers, M.; Vinckier, C. *J. Phys. Chem.* **1986**, *90*, 6552.

(4) Frank, P.; Bhaskaran, K. A.; Just, T. H. *21th Symp. (Int.) Combust.* **1986**, 885.

(5) Mahmud, K.; Fontijn, A. *J. Phys. Chem.* **1987**, *91*, 1918.

(6) Peeters, J.; Vanhaelemeersch, S.; Van Hoeymissen, J.; Borms, R.; Vermeylen, D. *J. Phys. Chem.* **1989**, *93*, 3892.

(7) Michael, J. V.; Wagner, A. F. *J. Phys. Chem.* **1990**, *94*, 2453 and references therein.

(8) Boullart, W.; Peeters, J. *J. Phys. Chem.* **1992**, *96*, 9810.

(9) Peeters, J.; Langhans, I.; Boullart, W. *Int. J. Chem. Kinet.* **1994**, *26*, 869.

(10) Huang, X.; Xing, G.; Bersohn, R. *J. Chem. Phys.* **1994**, *101*, 5818.

(11) Capozza, G.; Segoloni, E.; Leonori, F.; Volpi, G. G.; Casavecchia, P. *J. Chem. Phys.* **2004**, *120*, 4557.

(12) Chikan, V.; Leone, S. R. *J. Phys. Chem. A* **2005**, *109*, 2525.

(13) Harding, L. B. *J. Phys. Chem.* **1981**, *85*, 10.

(14) Harding, L.; Wagner, A. F. *J. Phys. Chem.* **1986**, *90*, 2974.

(15) From NIST web page: http://srdata.nist.gov/cccbdb/.

(16) Cicek, J. *J. Chem. Phys.* **1966**, *45*, 4256.

(17) Curtiss, L. A.; Raghavachari, K.; Redfern, P. C.; Rassolov, V.; Pople, J. A. *J. Chem. Phys.* **1998**, *109*, 7764.

(18) Montgomery, J. A., Jr.; Ochterski, J. W.; Petersson, G. A. *J. Chem. Phys.* **1994**, *101*, 5900.

(19) Bohn, B.; Stuhl, F. *J. Phys. Chem.* **1990**, *94*, 8010.

(20) Sheaffer, P. M.; Zittel, P. F. *J. Phys. Chem. A* **2000**, *104*, 10194.

(21) Baulch, D. L.; Cobos, C. J.; Cox, R. A.; Frank, P.; Hayman, G.; Just, Th.; Kerr, J. A.; Murrells, T.; Pilling, M. J.; Troe, J.; Walker, R. W.; Warnatz, J. *J. Phys. Chem. Ref. Data* **1994**, *23*, 847 and references therein.

(22) Melius, C. F. Unpublished; see ref 14.

(23) Girard, Y.; Chaquin, P. *J. Phys. Chem. A* **2003**, *107*, 10462.

(24) Becke, A. D. *J. Chem. Phys.* **1993**, *98*, 5648.

(25) Stevens, P. J.; Devlin, F. J.; Chablowski, C. F.; Frisch, M. J. *J. Phys. Chem.,* **1994**, *98*, 11623.

(26) Raghavachari, K.; Trucks, G. W.; Pople, J. A.; Head-Gordon, M. *Chem. Phys. Lett.* **1989**, *157*, 479.

(27) EMSL Basis Set Library, http://www.emsl.pnl.gov/forms/basis-form.html.

(28) Halkier, A.; Helgaker, T.; Jorgensen, P.; Klopper, W.; Koch, H.; Olsen, J.; Wilson, A. K. *Chem. Phys. Lett*. **1998**, *286*, 243.

(29) Möller, C.; Plesset, M. S. *Phys. Rev.* **1934**, *46*, 618.

(30) Head-Gordon, M.; Pople, J. A.; Frisch, M. J. *Chem. Phys. Lett.* **1988**, *153*, 503.

(31) Montgomery, J. A., Jr.; Frisch, M. J.; Ochterski, J. W.; Petersson, G. A. *J. Chem. Phys.* **1999**, *110*, 2822.

(32) Baboul, A. G.; Curtiss, L. A.; Redfern, P. C.; Raghavachari, K. *J. Chem. Phys.,* **1999**, *110*, 7650.

(33) Mebel, A. M.; Morokuma, K.; Lin, M. C. *J. Chem. Phys.* **1995**, *103*, 7414.

(34) Mayer, P. M.; Parkinson, C. J.; Smith, D. M.; Radom, L. *J. Chem. Phys.* **1998**, *108*, 604.

(35) Werner, H. J.; Knowles, P. J. *J. Chem. Phys.* **1985**, *82*, 5053.

(36) Knowles, P. J.; Werner, H. J. *Chem. Phys. Lett.* **1985**, *115*, 259.

(37) Gonzalez, C.; Schlegel, H. B. *J. Chem. Phys.* **1989**, *90*, 2154.

(38) Gonzalez, C.; Schlegel, H. B. *J. Phys. Chem.* **1990**, *94*, 5523.

(39) Frisch, M. J.; Trucks, G. W.; Schlegel, H. B.; Scuseria, G. E.; Robb, M. A.; Cheeseman, J. R.; Montgomery, J. A., Jr.; Vreven, T.; Kudin, K. N.; Burant, J. C.; Millam, J. M.; Iyengar, S. S.; Tomasi, J.; Barone, V.; Mennucci, B.; Cossi, M.; Scalmani, G.; Rega, N.; Petersson, G. A.; Nakatsuji, H.; Hada, M.; Ehara, M.; Toyota, K.; Fukuda, R.; Hasegawa, J.; Ishida, M.; Nakajima, T.; Honda, Y.; Kitao, O.; Nakai, H.; Klene, M.; Li, X.; Knox, J. E.; Hratchian, H. P.; Cross, J. B.; Bakken, V.; Adamo, C.; Jaramillo, J.; Gomperts, R.; Stratmann, R. E.; Yazyev, O.; Austin, A. J.; Cammi, R.; Pomelli, C.; Ochterski, J. W.; Ayala, P. Y.; Morokuma, K.; Voth, G. A.; Salvador, P.; Dannenberg, J. J.; Zakrzewski, V. G.; Dapprich, S.; Daniels, A. D.; Strain, M. C.; Farkas, O.; Malick, D. K.; Rabuck, A. D.; Raghavachari, K.; Foresman, J. B.; Ortiz, J. V.; Cui, Q.; Baboul, A. G.; Clifford, S.; Cioslowski, J.; Stefanov, B. B.; Liu, G.; Liashenko, A.; Piskorz, P.; Komaromi, I.; Martin, R. L.; Fox, D. J.; Keith, T.; Al-Laham, M. A.; Peng, C. Y.; Nanayakkara, A.; Challacombe, M.; Gill, P. M. W.; Johnson, B.; Chen, W.; Wong, M. W.; Gonzalez, C.; Pople, J. A. *Gaussian 03*, revision C.02; Gaussian, Inc.: Wallingford, CT, 2004.

(40) Helgaker, T.; Jensen, H. J. Aa.; Joergensen, P.; Olsen, J.; Ruud, K.; Aagren, H.; Auer, A. A.; et al. DALTON, a molecular electronic structure program, Release 1.2; 2001.

(41) Werner, H.-J.; Knowles, P. J.; Schütz, M.; Lindh, R.; Celani, P.; Korona, T.; Rauhut, G.; Manby, F. R.; Amos, R. D.; Bernhardsson, A.; Berning, A.; Cooper, D. L.; Deegan, M. J. O.; Dobbyn, A. J.; Eckert F.; et al. MOLPRO is a package of ab initio programs; 2002.

(42) Gillespie, D. T. *J. Comput. Phys.* **1976**, *22*, 403.

(43) Gillespie, D. T. *J. Phys. Chem.* **1977**, *81*, 2340.

(44) Gillespie, D. T. *J. Comput. Phys.* **1978**, *28*, 395.

(45) Vereecken, L.; Huyberechts, G.; Peeters, J. *J. Chem. Phys.* **1997**, *106*, 6564.

(46) Matsumoto, M.; Nishimura, T. *ACM Trans. Model. Comput. Simul.* **1998**, *8*, 3.

(47) Hippler, H.; Troe, J.; Wendelken, H. J. *J. Chem. Phys.* **1983**, *78*, 6709.

(48) Troe, J. *J. Chem. Phys.* **1977**, *66*, 4745.

(49) Forst, W. *Theory of Unimolecular Reactions*; Academic Press: New York, 1973.

(50) Robinson, P.; Holbrook, K. *Unimolecular Reactions*; Wiley-Interscience: London, 1972.

(51) Gilbert, R. G.; Smith, C. S. *Theory of Unimolecular and Recombination Reactions*; Blackwell Scientific: Oxford, U.K., 1990.

(52) Holbrook, K.; Pilling, M.; Robertson, S. *Unimolecular Reactions*, 2nd ed.; Wiley: New York, 1996.

(53) Steinfeld, J. I.; Francisco, J. S.; Hase, W. L. *Chemical Kinetics and Dynamics*; Prentice Hall: Englewood Cliffs, NJ, 1999.

(54) Baer, T.; Hase, W. L. *Unimolecular Reaction Dynamics: Theory and Experiment*; Oxford University Press: Oxford, U.K., 1996.

(55) Beyer, T.; Swinehart, D. F. *Comm. Assoc. Comput. Machines* **1973**, *16*, 379.

(56) Stein, S. E.; Rabinovitch, B. S. *J. Chem. Phys.* **1973**, *58*, 2438.

(57) Malick, D. K.; Petersson, G. A.; Montgomery, J. A., Jr. *J. Chem. Phys.* **1998**, *108*, 5704.

(58) Miller, W. H. *J. Am. Chem. Soc.* **1979**, *101*, 6810.

(59) Peeters, J.; Devriendt, K. *21th Symp. (Int.) Combust.* **1996**, 1001.

(60) Nguyen, T. L.; Vereecken, L.; Hou, X. J.; Nguyen, M. T.; Peeters, J. *J. Phys. Chem. A* **2005**, *109*, 7489.

(61) Nguyen, T. L.; Dils, B.; Carl, S. A.; Vereecken, L.; Peeters, J. *J. Phys. Chem. A* **2005**, *109*, 9786.

(62) Marcus, R. A. *J. Chem. Phys.* **1966**, *45*, 2138.

(63) Marcus, R. A. *J. Chem. Phys.* **1967**, *46*, 959.

(64) Morokuma, K.; Eu, B. C.; Karplus, M. *J. Chem. Phys.* **1969**, *51*, 5193.

(65) Lin, S. H.; Lau, K. H.; Eyring, H. *J. Chem. Phys.* **1971**, *55*, 5657.

(66) NIST web page: http://physics.nist.gov/PhysRefData/Handbook/periodictable.htm.

(67) Mordaunt, D. H.; Osborn, D. L.; Choi, H.; Bise, R. T.; Neumark, D. M. *J. Chem. Phys.* **1996**, *105*, 6078.

(68) Choi, H.; Mordaunt, D. H.; Bise, R. T.; Taylor, T. R.; Neumark, D. M. *J. Chem. Phys.* **1998**, *108*, 4070.

(69) Scott, A. P.; Radom, L. *J. Phys. Chem.* **1996**, *100*, 16502.